Nikolayev, V. S. & Sundararaj, S. Oscillating menisci and liquid films at evaporation/condensation, Heat Pipe Science and Technology, 2014 vol. 5(1-4), 59 - 67.

OSCILLATING MENISCI AND LIQUID FILMS AT EVAPORATION/CONDENSATION

Vadim Nikolayev[1]*, **Senthilkumar Sundararaj**[2]†

[1]Service de Physique de l'Etat Condensé (CNRS URA 2464), IRAMIS/CEA Saclay, 91191 Gif-sur-Yvette Cedex, France

[2]CEA-INAC/SBT, UMR E9004 CEA-UJF Grenoble, 38054 Cedex 9, France

ABSTRACT To understand the functioning of the pulsating heat pipe (PHP), a liquid film formed by a unique oscillating meniscus is studied under evaporation or condensation conditions within a 2D numerical approach based on the lubrication approximation. The transient heat and mass transfer problem coupled with hydrodynamics is solved within a Taylor bubble hydrodynamics problem. A simple expression for the film thickness time evolution is obtained as a function of the meniscus velocity among other parameters. The time evolution of the meniscus shape is calculated. Based on it, the heat and mass exchange at the gas-liquid interface is evaluated. The contributions of both flat film and curved portion of the gas-liquid interface to the overall heat transfer are analyzed. A criterion defining whether the film is flat or wedge-like, is proposed.

KEYWORDS: PHP, liquid film, oscillation, Taylor bubble

1. INTRODUCTION

The pulsating (or oscillating) heat pipe (PHP) is a long capillary tube bent into many branches and partially filled with a two-phase, usually single component, working fluid [Akachi, 1993]. During PHP functioning, a moving pattern of multiple vapor bubbles separated by liquid plugs forms spontaneously inside the tube. Because of their simplicity and high performance, PHPs are often considered as highly promising. Their industrial application is however limited because the functioning of PHPs is not completely understood.

During the last decade, researchers have extensively studied PHPs [Zhang and Faghri, 2008; Khandekar et al., 2010]. The main flow pattern inside the PHP is the slug flow, i.e. the flow of the "Taylor bubbles" where the gas is surrounded by thin liquid films. A major part of mass exchange occurs on their interface with the vapor like in the conventional heat pipes. Since the mass exchange provides both a moving force for the oscillations and a heat exchange, the films are extremely important for the PHP functioning. A special care should thus be taken in order to predict correctly the film length and thickness. Their first description was provided by Zhang and Faghri [2002], who introduced static wetting films, the thickness of which was controlled by the intermolecular forces introduced via disjoining pressure. The films were thus nanometric like in conventional heat pipes. It is however well known that the thickness of the Taylor bubble films is controlled by a hydrodynamic phenomenon, depends on the meniscus velocity, and is usually micrometric [Bretherton, 1961]. The thickness scaling with velocity is similar to the phenomenon of Landau and Levich [1942]. While the Landau-Levich films have been extensively investigated in the isothermal and constant meniscus velocity situation, their studies for cases where the phase change or transient effects are involved, are rare. Lagubeau [2006] observed successive events of film deposition by the receding meniscus and film drying in such a way that the film length varied during the meniscus oscillations. Das et al. [2010]; Nikolayev [2011, 2013] accounted for the varying film length in the PHP modeling. The film thickness in their model was assumed however to be constant.

*Corresponding author: vadim.nikolayev@cea.fr

†Present address: Dept. of Aeronautical Engineering, Vel Tech Dr. RR & Dr. SR Technical University, Chennai, India

Since the PHP films are not well understood we will begin their study here with a very simplified case where the triple contact line effects are neglected. The objective of the present paper is to introduce a theory of hydrodynamically controlled films, calculate their spatial and temporal thickness variation during meniscus oscillations and study the impact of the varying film on the overall heat transfer at either permanent evaporation or permanent condensation.

2. PROBLEM FORMULATION

A gas bubble moves with a velocity $\vec{U}$ in a capillary tube filled with an incompressible Newtonian liquid. The bubble has a length much larger than the tube radius so that a unique meniscus may be studied. The reference of the meniscus will be considered hereafter in which the tube walls move with the velocity $-\vec{U}$. The gas is the pure liquid vapor. The effect of gravity is neglected and the gas-liquid interface is thus symmetric (Fig. 1). Both the liquid-vapor and liquid-solid interfaces are assumed to be isothermal. The background argument is that the temperature of the liquid-vapor interface is generally equal to the saturation temperature T_s corresponding to the given vapor pressure. On the other hand, the internal wall of the tube is isothermal due to its high thermal conductivity. The wall temperature is $T_w = T_s - \Delta T$, where ΔT is the wall subcooling.

The following assumptions are made in the present work. The interface is cut into two parts depending on the h/R value (where $h = h(x)$ is the liquid layer thickness, cf. Fig. 1): the film region at $x < x_c$ and the remaining part of the interface at $x > x_c$. While the film behavior is controlled by the viscous stresses, they are relatively unimportant in the determination of the macroscopic meniscus shape that is controlled mainly by the surface tension. For this reason, a contribution of the viscous and inertial effects on the interface shape is neglected so that the apparent meniscus curvature is spatially constant and this region is called a capillary static region. On one hand, x_c should be close enough to x_m, the abscissa of bubble tip, so that the curvature already does not vary at x_c and the evaporation is negligible there. On the other hand, the film slope should be small enough so that we can apply the lubrication approximation [Oron et al., 1997]. Within such an approximation, $h(x_c)/R$ is small so that the film curvature in the azimuthal direction is neglected and the film may be considered to be two dimensional.

"One sided model" is adopted in which the vapor pressure p_V is assumed to be spatially homogeneous. This hypothesis is justified by the smallness of both density and viscosity of the vapor with respect to those of the liquid. The vapor is assumed to be insulating and the heat flux to the vapor domain can be neglected. This leads to the interfacial energy balance

$$\mathcal{L}J = q_{int}, \tag{1}$$

where J is the interfacial mass flux due to condensation/evaporation ($J > 0$ at condensation) and the interfacial heat flux q_{int} from the liquid side is positive when directed toward the liquid (along the normal $\vec{n}$, cf. Fig. 1).

The temperature distribution in the liquid film is assumed to be stationary (i.e., linear in y). This approximation is valid when the liquid film thickness is smaller than the thermal diffusion characteristic length. The heat flux inside the liquid is then independent of y so that

$$q_{int} = k_L \frac{T_{int} - T_w}{h}. \tag{2}$$

The combination of Eqs. (1) and (2) results in

$$J = \frac{k_L \Delta T}{h\mathcal{L}}. \tag{3}$$

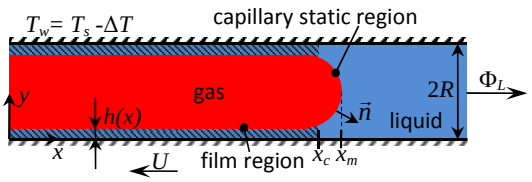

FIG. 1 : Problem geometry

2.1 Conservation of mass

Since liquid is incompressible, the liquid mass conservation means its volume conservation. The volume flux Φ (per unit length in the azimuthal direction) flowing through the film at a given position x is

$$\Phi = \int_0^{h(x)} v_x dy, \tag{4}$$

where v_x is the x component of the liquid velocity. The volume conservation states that the sum of $\Phi = \Phi(x)$ and of the volume flux due to condensation equals the total volume flux Φ_L at the right end of the tube. This equality is expressed by the following relation valid at any $x \leq x_c$,

$$\Phi(x) + \int_x^{x_m} v_n(x')dx' = \Phi_L. \tag{5}$$

Here v_n represents a projection of the interfacial liquid velocity to the vector $\vec{n}$ normal to the interface and directed toward the liquid.

At $x \to -\infty$ (far from the moving meniscus), the liquid film is immobile with respect to the wall because there is no pressure gradient inside it, $v_x = -U$ and $\Phi(-\infty) = -Uh(-\infty)$. One obtains from (5) that

$$\Phi_L = \int_{-\infty}^{x_m} v_n(x')dx' - Uh(-\infty) \tag{6}$$

is independent of $x > x_m$. By using (6) in (5) one finally obtains the mass conservation law in the direction parallel to the wall,

$$\Phi(x) = -Uh(-\infty) + \int_{-\infty}^{x} v_n(x)dx. \tag{7}$$

The latter expression can be rewritten as

$$v_n = \partial\Phi/\partial x. \tag{8}$$

The mass conservation at the gas-liquid interface implies that [Nikolayev, 2010]

$$J = (v_n - v_{int})\rho_L \tag{9}$$

where

$$v_{int} = -\partial h/\partial t \tag{10}$$

is the interface velocity projection to $\vec{n}$ in the lubrication (small interface slope) approximation.

2.2 Governing equations

The no-slip condition imposed at the tube wall and no-tangential stress boundary condition at the free interface reads

$$v_x = -U \quad \text{at} \quad y = 0, \tag{11}$$

$$\partial v_x/\partial y = 0 \quad \text{at} \quad y = h(x). \tag{12}$$

The Stokes equations in lubrication approximation [Nikolayev, 2010] with these boundary conditions result in the following expression obtained with the definition (4)

$$\Phi = -\frac{h^3}{3\mu}\frac{\partial p_L}{\partial x} - Uh, \tag{13}$$

where p_L is the liquid pressure. Within the lubrication approximation and in the absence of gravity it is constant across the liquid film. The normal stress boundary condition in the lubrication approximation is

$$\Delta p \equiv p_V - p_L = \sigma\frac{\partial^2 h}{\partial x^2}, \tag{14}$$

where the vapor pressure p_V is independent of x as mentioned above.

By substituting Eqs. (3, 9, 10) and (13-14) into Eq. (8) one arrives to the following expression for the evolution of the film thickness

$$\frac{\partial h}{\partial t} + \frac{\partial}{\partial x}\left(\frac{\sigma}{3\mu}h^3\frac{\partial^3 h}{\partial x^3} - Uh\right) = \frac{k_L \Delta T}{h\mathcal{L}\rho_L}. \tag{15}$$

The difficulty of solution of the governing equations (14, 15) is that their solution does not exist for arbitrary boundary conditions which should thus be chosen carefully from the analysis of their form.

Let us use the following conversion to the dimensionless variables: $x = h_0 Ca_0^{1/3}\lambda$, $h = h_0 Ca_0^{2/3}\tilde{h}$, $t = h_0\mu\sigma^{-1}Ca_0^{-2/3}\tau$, $U = U_0\tilde{U}$ (where the reference values $U_0 > 0$ and h_0 will be both defined later on). The dimensionless governing equation reads

$$\frac{\partial \tilde{h}}{\partial \tau} + \frac{\partial}{\partial \lambda}\left(\frac{\tilde{h}^3}{3}\frac{\partial^3 \tilde{h}}{\partial \lambda^3} - \tilde{U}\tilde{h}\right) = \frac{N}{\tilde{h}}. \tag{16}$$

Two dimensionless groups are introduced here: the capillary number $Ca_0 = \mu U_0/\sigma$ and the evaporation-condensation number

$$N = \frac{k_L \Delta T \mu}{\mathcal{L}\rho_L \sigma h_0 Ca_0^2}.$$

2.3 Flat or wedge shaped film?

There is an interesting conclusion that may be deduced from Eq. (16). The variables are normalized there in a unique way that makes the velocity amplitude disappear from the equation. One may thus reasonably state that the time $t_{rel} = h_0\mu\sigma^{-1}Ca_0^{-2/3}$ used for this purpose is the characteristic time of relaxation of a film deformation. On the other hand, by comparing the first and the last terms of Eq. (15), it becomes evident that the time $t_{ec} = h_0^2 Ca_0^{4/3}\mathcal{L}\rho_L/(k_L|\Delta T|)$ characterizes the evaporation/condensation rate; $|N| = t_{rel}/t_{ec}$. For this reason, the number $|N|$ may be used to characterize the film shape during the meniscus receding. At $|N| > 1$, the film is expected to be wedge-shaped like Chauris et al. [2013] assumed it, because the earlier deposed film portions have already smaller thickness than the newly deposed film. At $|N| \ll 1$, $t_{rel} \ll t_{ec}$ and the fast film shape relaxation leads to the flat film.

3. BOUNDARY CONDITIONS

3.1 Stationary receding

In the isothermal ($\Delta T = 0$, $N = 0$) case, there are stationary solutions of Eq. (16). Let us consider the stationary receding solution $\tilde{h} = \tilde{h}_r(\lambda)$ first, which is a classical Landau and Levich problem. By choosing the meniscus receding velocity $U_r = U_0$, one obtains $\tilde{U} = 1$; no more parameters remain in the equation. The film thickness at infinity [Landau and Levich, 1942; Bretherton, 1961]

$$h_r(x \to -\infty) \equiv h_\infty = h_0 Ca_r^{2/3}, \tag{17}$$

where $Ca_r = \mu U_r/\sigma$, may be used to introduce yet unknown h_0. The first boundary condition in the dimensionless form thus reads

$$\tilde{h}|_{\lambda\to-\infty} = 1. \tag{18}$$

At $\lambda \to -\infty$, $\Phi \to -Uh$, $\partial^3\tilde{h}/\partial\lambda^3 \to 0$, and Eq. (16) can be integrated once resulting in the equation

$$\tilde{h}^3\frac{\partial^3\tilde{h}}{\partial\lambda^3} = 3(\tilde{h} - 1). \tag{19}$$

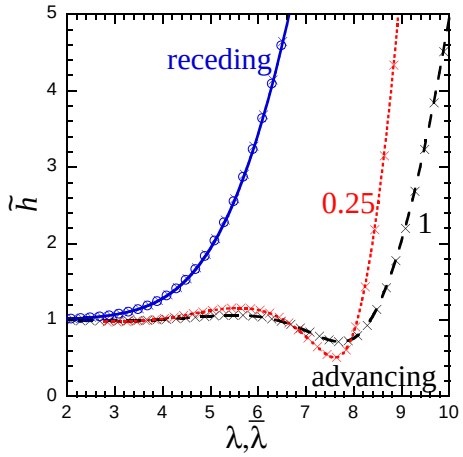

FIG. 2 : Stationary film profiles for the receding ($\tilde{h}_r(\lambda)$, blue solid line) and advancing ($\tilde{h}_a(\bar{\lambda})$) menisci obtained with shooting. For the latter, the shapes calculated for $Ca_a/Ca_r = 1$ (black dashed line) and 0.25 (red dotted line) are presented. The crosses show the respective shooting results obtained with the zero initial conditions for the derivatives. The circles show $\tilde{h}_r(\lambda)$ calculated with FDM.

Landau and Levich [1942] and Bretherton [1961] found that its asymptotics at $\lambda \to -\infty$ reads

$$\tilde{h}_r = 1 + \varepsilon \exp\left(3^{1/3}\lambda\right), \tag{20}$$

where ε is a constant. At $\lambda \to \infty$ the solution of Eq. (19) approaches a constant curvature curve (a parabola in the lubrication approximation), i.e. the meniscus in the capillary static region. The curvature matching condition (one neglects here the film thickness with respect to R)

$$R^{-1} = \alpha/h_0, \tag{21}$$

where $\alpha = \partial^2\tilde{h}_r/\partial\lambda^2|_{\lambda\to\infty}$, defines h_0.

One can calculate α numerically by fixing initial conditions at some $\lambda = \lambda_0$. Since ε does not influence the solution (its change leads simply to a shift of the $\tilde{h}_r(\lambda)$ curve along the λ axis), one can choose $\lambda_0 = 0$ so that one obtains the boundary condition

$$\tilde{h}(\lambda = 0) = 1 + \varepsilon. \tag{22}$$

Other two initial conditions may be obtained from (20) by its differentiation. The Eq. (19) numerical solution results in $\alpha = 1.3375 \pm 10^{-4}$. According to Eq. (21), $h_0 = \alpha R$. The solution $\tilde{h} = \tilde{h}_r(\lambda)$ is shown in Fig. 2.

Since the film thickness is neglected in the meniscus curvature estimation (R^{-1}), there is a small correction [Aussillous and Quéré, 2000] to Eq. (17). The resulting formula describes well the experimental data [Tibiriçá et al., 2010; Han and Shikazono, 2009]. This formula derived initially for the Stokes flow (zero Reynolds number), works well [Kreutzer et al., 2005] for moderate Reynolds numbers < 100 characteristic of the PHP flow.

It is important to mention that the existence of the film considered here depends on the wetting properties of the capillary. For small contact angles (wetting case), the films always appear because when the receding motion begins, the triple contact line is easily pinned at surface defects and the film forms immediately. For large contact angles (less wettable surface), the contact line is not pinned at cleaned surfaces; the film appears only for $Ca \gtrsim 10^{-2}$, i.e. above the dynamic wetting transition [Delon et al., 2008]. This means that for good PHP functioning one wants to use the well wettable tubes.

3.2 Stationary advancing

Let the meniscus change the direction and advance with a constant velocity $U = -U_a < 0$ over the already pre-formed film of the thickness given by Eq. (17). By introducing $\bar{\lambda} = Ca_a^{1/3}x/h_\infty$, where $Ca_a = \mu U_a/\sigma$,

one obtains the equation for $\tilde{h} = \tilde{h}_a(\bar{\lambda})$

$$\tilde{h}^3 \frac{\partial^3 \tilde{h}}{\partial \bar{\lambda}^3} = 3(1 - \tilde{h}). \tag{23}$$

Like in the previous case, the curvature saturates at $\bar{\lambda} \to \infty$ and the curvature matching results in [Maleki et al., 2011]

$$\partial^2 \tilde{h}_a / \partial \bar{\lambda}^2 |_{\bar{\lambda} \to \infty} = \alpha (Ca_r / Ca_a)^{2/3}. \tag{24}$$

The asymptotics at $\bar{\lambda} \to -\infty$ is [Bretherton, 1961]

$$\tilde{h}_a = 1 + \bar{\varepsilon} \exp[3^{1/3}(\bar{\lambda} - \bar{\lambda}_0)/2] \cos[3^{5/6}(\bar{\lambda} - \bar{\lambda}_0)/2], \tag{25}$$

where $\bar{\varepsilon}$, $\bar{\lambda}_0$ are constants. While $\bar{\lambda}_0$ reflects the invariance of the solution with respect to the translation along the $\bar{\lambda}$ axis (and may be chosen arbitrarily but large enough to provide the asymptotics validity), $\bar{\varepsilon}$ depends on the curvature of the $\tilde{h}_a(\bar{\lambda})$ curve at $\bar{\lambda} \to \infty$. It is determined by numerical shooting to the condition (24). The initial conditions may be obtained from (25) by its differentiation. According to Eq. (25), the film thickness exhibits undulations (Fig. 2), the (dimensional) period of which is $\simeq 6.73 R Ca_a^{-1/3} Ca_r^{2/3}$. It was shown by Maleki et al. [2011] that such a theory agrees with experiments for the flat film geometry. For the Taylor bubble geometry, these undulations were evidenced by Lips et al. [2010] among others.

3.3 Insensitivity to the boundary conditions

It was shown above that the boundary conditions are found from the asymptotic solutions. It would be difficult however to find the asymptotics in the transient case. It turns out that it is possible to use the boundary conditions common for both receding and advancing situations in the form (22) together with the zero values for both the first and the second derivatives of $\tilde{h}$ at $\lambda = 0$ with no loss of accuracy (Fig. 2). The difference between the receding and advancing cases is that the value of ε is arbitrary (but small) for receding and should be adjusted to provide the curvature (24) for advancing. Such an insensitivity to the form of the boundary conditions is explained by the stability of solutions: in spite of the weak initial deviation, the numerical algorithm does not deviate from them. Such a feature permits the use of the zero initial conditions in the transient case for arbitrary velocity.

The shooting can only be used for the stationary case. In the transient case, a finite difference numerical method (FDM) needs to be applied to solve Eq. (16) (see Fig. 2 for the h_r FDM result). In this case we used the following boundary conditions at $\lambda = 0$: $\tilde{h} = 1$ and $\partial^2 \tilde{h} / \partial \lambda^2 = 0$. Both the curvature

$$\partial^2 \tilde{h} / \partial \lambda^2 |_{\lambda = \lambda_c} = \alpha \tag{26}$$

and the height $\tilde{h}_c$ need to be specified at $\lambda = \lambda_c$. Without any loss of generality we chose $\lambda_c = 80$, $\tilde{h}_c = 20$.

3.4 Phase change case

Let us assume that at $t = 0$, the stationary Landau-Levich profile discussed in the section 3.1 is established and a nonzero value of ΔT is imposed at $t = 0$, i.e. $\tilde{h}(\tau = 0, \lambda) = \tilde{h}_r(\lambda)$. The phase change starts. It is evident that, similarly to the stationary case, there is no flow at $\lambda = 0$ with respect to the wall when the phase change occurs; the interface evolution is entirely due to the phase change. The interface remains thus flat and its evolution may be obtained directly from Eq. (16) by putting to zero the spatial derivatives,

$$\tilde{h}(\tau, \lambda = 0) = \sqrt{2N\tau + 1}. \tag{27}$$

For the phase change case, Eq. (27) replaces the condition $\tilde{h}(\lambda = 0) = 1$. The matching condition (26) remains the same as in the isothermal case.

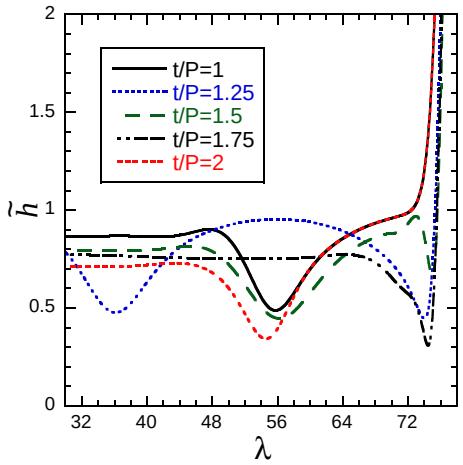

FIG. 3 : Meniscus shape variation over one period of oscillations for $N = -9.8 \cdot 10^{-4}$ corresponding to $\Delta T = -5°$ (evaporation case).

4. HEAT FLUX CALCULATION

The heat exchange rate may be calculated as

$$Q \simeq 2\pi R \int_{x_c - L}^{x_c} q_{int}(x) dx, \tag{28}$$

where the contribution of the capillary static region is neglected. One can see that Q depends on the liquid film length L. Far from the meniscus, the film thickness saturates at $h(x \to -\infty)$ given by Eq. (27), and $q_{int} \to k_L \Delta T / h(x \to -\infty)$. To reveal the effect of the meniscus curvature, one can subtract this ("flat film") part

$$Q_f = 2\pi R L k_L \Delta T / h(x \to -\infty) \tag{29}$$

from $Q = Q_m + Q_f$. The remaining ("meniscus") part

$$Q_m = 2\pi R k_L \Delta T \int_{x_c - L}^{x_c} \left[\frac{1}{h(x)} - \frac{1}{h(x \to -\infty)} \right] dx. \tag{30}$$

is independent of L when it is large enough. Note that this division to the flat film and meniscus parts corresponds exactly to the analogous division performed in the PHP film evaporation-condensation model [Das et al., 2010; Nikolayev, 2011, 2013].

5. RESULTS AND DISCUSSION

When the meniscus oscillates, so that $x_c = L_0 \sin(2\pi t/P)$, the meniscus velocity is $U = \dot{x}_c = U_0 \cos(2\pi t/P)$, where $U_0 = 2\pi L_0/P$ is a reference value to be used for both the Ca_0 calculation and the initial condition (stationary receding profile for $U_r = U_0$). Since the film appears when deposed by the receding meniscus, $L = 0$ when the meniscus is at its far left position $-L_0$. Without a contact line modeling, one cannot calculate the velocity of its retraction as it was done e.g. by Nikolayev [2010]. We assume instead that, in the tube reference, the film edge is immobile because of its pinning on a surface heterogeneity. The film length is then $x_c + L_0$, i.e.

$$L = L_0[1 + \sin(2\pi t/P)]. \tag{31}$$

The dimensionless velocity reads $\tilde{U} = \cos(2\pi\tau/\tilde{P})$, where $\tilde{P} = P\sigma(h_0\mu)^{-1}Ca_0^{2/3}$.

Within such a problem statement, the meniscus dynamics is determined by only two dimensionless numbers N, $\tilde{P}$. Ethanol at 1 bar, $L_0 = 5$ mm, $R = 1$ mm, and $P = 0.25$ s was chosen for simulation, for which $\tilde{P} \simeq 125$, $Ca_0 \simeq 6.6 \cdot 10^{-3}$. The film shape evolution is shown in Fig. 3. The film is wavy. Its thinnest point is located close to the meniscus. Similar to the stationary advancing case considered above, the waves appear because of

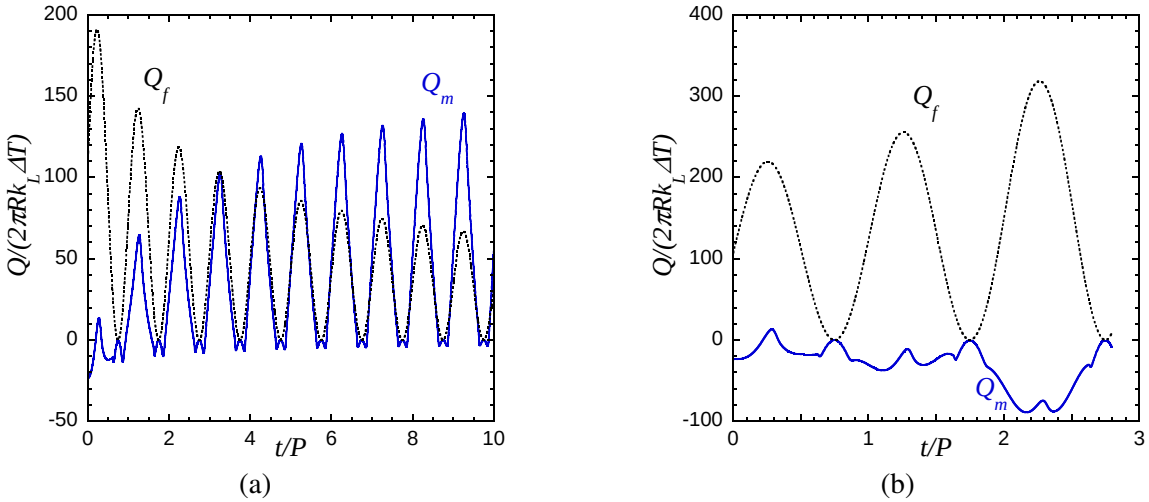

FIG. 4 : Heat exchange (a) at condensation for $N = 3.9 \cdot 10^{-3}$ corresponding to $\Delta T = 20°$ and (b) at evaporation for the same parameters as Fig. 3.

a mismatch of the film thickness and the meniscus velocity. At evaporation, the film thins until it eventually disrupts at a point of minimal thickness, for the case of Fig. 3, at $\lambda \approx 75$. The simulation then ends.

The heat exchange rate time evolutions for condensation and evaporation are shown in Figs. 4. At evaporation, the heat exchange is mainly defined (cf. Fig. 4b) by the flat film contribution Q_f that may be easily found with Eq. (27). At condensation, at the early times, the heat exchange is also defined by Q_f. Later on, the film thickness grows and Q_f decreases, cf. Fig. 4a. The contribution Q_m of the wavy thickness variation (where the flux is larger at points where the thickness is smaller) becomes more important. Note that in the PHP, the time during which the film is continuously located in the evaporator or in the condenser, may vary from a fraction to several oscillation periods so that the above consideration does make sense.

The theory presented here is complicated and its implications for the PHPs need to be identified now. Some results obtained here (film flatness for $|N| \ll 1$, film thickness evolution (27)) may be directly used in the PHP simulation. An important question concerning the film length in the evaporator however remains open. This article is a first approach to this important question. It was assumed here that the contact line (where the film ends) is pinned and does not move at all. In the earlier models Das et al. [2010]; Nikolayev [2011, 2013], it was assumed that the film thickness does not change and the contact line receding dynamics is given by the film mass decrease. The reality is somewhere in between. A rigorous description of the contact line effects [Nikolayev, 2010] needs to be introduced into the present model to simulate a more realistic film length dynamics.

ACKNOWLEDGMENTS

A financial support of ANR in the framework of the project AARDECO ANR-12-VPTT-005-02 and of CEA in the framework of the project NTE COSOL is acknowledged.

NOMENCLATURE

Ca	capillary number
h	interface height [m]
k	heat conductivity [W/(m·K)]
L	liquid film length [m]
P	oscillation period [s]
p	pressure [Pa]
Q	heat exchange rate [W]
q	heat flux [W/m^2]
R	tube radius [m]
T	temperature [K]
t	time [s]
U, v	velocity [m/s]
x, y	coordinates [m]
$\mathcal{L}$	latent heat [J/kg]

Greek symbols

λ	dimensionless x

μ	liquid shear viscosity [Pa·s]	f	film
Φ	volume liquid flux per tube perimeter [m^2/s]	int	interface
ρ	liquid density [kg/m^3]	L	liquid
σ	surface tension [N/m]	m	meniscus
τ	dimensionless t	n	component normal to the interface
		r	receding
Subscripts and superscripts		s	saturation
0	reference value	V	vapor
a	advancing	w	internal tube wall

REFERENCES

Akachi, H., "Structure of micro-heat pipe," US Patent 5219020 (1993).

Aussillous, P. and Quéré, D., "Quick deposition of a fluid on the wall of a tube," Phys. Fluids, 12(10), pp. 2367 – 2371 (2000).

Bretherton, F. P., "The motion of long bubbles in tubes," J. Fluid Mech., 10, pp. 166 – 188 (1961).

Chauris, N., Bonnenfant, J.-F., Ayel, V., Romestant, C. and Bertin, Y., "About the relevance of local IR visualization on tube walls of pulsating heat pipes: A modeling investigation," in "Proc. 17th Int. Heat Pipe Conf.", Kanpur, India: IIT Kanpur (2013).

Das, S. P., Nikolayev, V. S., Lefèvre, F., Pottier, B., Khandekar, S. and Bonjour, J., "Thermally induced two-phase oscillating flow inside a capillary tube," Int. J. Heat Mass Transfer, 53(19-20), pp. 3905 – 3913 (2010).

Delon, G., Fermigier, M., Snoeijer, J. H. and Andreotti, B., "Relaxation of a dewetting contact line. Part 2: Experiments," J. Fluid Mech., 604, pp. 55 – 75 (2008).

Han, Y. and Shikazono, N., "Measurement of the liquid film thickness in micro tube slug flow," Int. J. Heat Fluid Flow, 30(5), pp. 842 – 853 (2009).

Khandekar, S., Panigrahi, P. K., Lefèvre, F. and Bonjour, J., "Local hydrodynamics of flow in a pulsating heat pipe: a review," Frontiers in Heat Pipes, 1(2), p. 023003 (2010).

Kreutzer, M. T., Kapteijn, F., Moulijn, J. A., Kleijn, C. R. and Heiszwolf, J. J., "Inertial and interfacial effects on pressure drop of Taylor flow in capillaries," AlChE J., 51(9), pp. 2428 – 2440 (2005).

Lagubeau, G., Propulsion par moteur pop-pop, Master's thesis, supervisor: D. Quéré, PMMH-ESPCI, Paris (2006).

Landau, L. D. and Levich, B. V., "Dragging of a liquid by a moving plate," Acta physico-chimica USSR, 17, pp. 42 – 54 (1942).

Lips, S., Bensalem, A., Bertin, Y., Ayel, V., Romestant, C. and Bonjour, J., "Experimental evidences of distinct heat transfer regimes in pulsating heat pipes (PHP)," Appl. Therm. Eng., 30(8-9), pp. 900 – 907 (2010).

Maleki, M., Reyssat, M., Restagno, F., Quéré, D. and Clanet, C., "Landau-Levich menisci," J. Colloid Interface Sci., 354(1), pp. 359 – 363 (2011).

Nikolayev, V. S., "Dynamics of the triple contact line on a nonisothermal heater at partial wetting," Phys. Fluids, 22(8), p. 082105 (2010).

Nikolayev, V. S., "A dynamic film model of the pulsating heat pipe," J. Heat Transfer, 133(8), p. 081504 (2011).

Nikolayev, V. S., "Oscillatory instability of the gas-liquid meniscus in a capillary under the imposed temperature difference," Int. J. Heat Mass Transfer, 64, pp. 313 – 321 (2013).

Oron, A., Davis, S. H. and Bankoff, S. G., "Long-scale evolution of thin liquid films," Rev. Mod. Phys., 69(3), pp. 931–980 (1997).

Tibiriçá, C. B., do Nascimento, F. J. and Ribatski, G., "Film thickness measurement techniques applied to micro-scale two-phase flow systems," Exp. Therm Fluid Sci., 34(4), pp. 463 – 473 (2010).

Zhang, Y. and Faghri, A., "Heat transfer in a pulsating heat pipe with open end," Int. J. Heat Mass Transfer, 45(4), pp. 755 – 764 (2002).

Zhang, Y. and Faghri, A., "Advances and unsolved issues in pulsating heat pipes," Heat Transfer Eng., 29(1), pp. 20 – 44 (2008).